







Article

Deactivation of a Pd/Pt Bimetallic Oxidation Catalyst Used in a Biogas-Powered Euro VI Heavy-Duty Engine Installation

Johanna Englund ^{1,*} , Kunpeng Xie ² , Sandra Dahlin ³ , Andreas Schaefer ¹ ,
Dazheng Jing ², Soran Shwan ², Lennart Andersson ², Per-Anders Carlsson ¹ ,
Lars J. Pettersson ³ and Magnus Skoglundh ¹ 

¹ Competence Centre for Catalysis, Department of Chemistry and Chemical Engineering, Chalmers University of Technology, 41296 Gothenburg, Sweden; andreas.schaefer@chalmers.se (A.S.); per-anders.carlsson@chalmers.se (P.-A.C.); skoglundh@chalmers.se (M.S.)

² Volvo Group Trucks Technology, 41296 Gothenburg, Sweden; kunpeng.xie@volvo.com (K.X.); dazheng.jing@volvo.com (D.J.); soran.shwan@volvo.com (S.S.); lennart.la.andersson@volvo.com (L.A.)

³ Department of Chemical Engineering, KTH Royal Institute of Technology, 00000 Stockholm, Sweden; sanj@kth.se (S.D.); lpet@kth.se (L.J.P.)

* Correspondence: johanna.englund@chalmers.se; Tel.: +46-31-772-2925

Received: 9 October 2019; Accepted: 28 November 2019; Published: 2 December 2019



Abstract: The reduction of anthropogenic greenhouse gas emissions is crucial to avoid further warming of the planet. We investigated how effluent gases from a biogas powered Euro VI heavy-duty engine impact the performance of a bimetallic (palladium and platinum) oxidation catalyst. Using synthetic gas mixtures, the oxidation of NO, CO, and CH₄ before and after exposure to biogas exhaust for 900 h was studied. The catalyst lost most of its activity for methane oxidation, and the activity loss was most severe for the inlet part of the aged catalyst. Here, a clear sintering of Pt and Pd was observed, and higher concentrations of catalyst poisons such as sulfur and phosphorus were detected. The sintering and poisoning resulted in less available active sites and hence lower activity for methane oxidation.

Keywords: oxidation catalyst; emission control; catalyst deactivation; engine bench; biogas; methane

1. Introduction

To mitigate the negative impacts of emissions on health and the environment from the transportation sector, emission legislation is applied around the world. The legislation regulates the emission levels of nitrogen oxides (NO_x), particulate matter (PM), carbon monoxide (CO), and hydrocarbons (HC). Regulations restricting the emissions of CO₂ will be more common and are already in place in some parts of the world [1]. The emissions from a vehicle must not exceed certain levels over the lifetime of the vehicle or a certain distance of use, which for heavy-duty vehicles in Europe presently is seven years or 700,000 km, respectively [2]. There are several approaches toward the reduction of CO₂ emissions from vehicles. One of these approaches is to increase the efficiency of the engine to reduce the amount of fuel that is used. However, a more efficient engine could lead to a reduction in exhaust temperature. This will put more pressure on the development of catalytic materials that have higher efficiency at lower temperatures, to be able to comply with regulations [3]. Another approach to reduce the emissions of fossil CO₂ to the atmosphere is to increase the use of biofuels such as biogas. One possible disadvantage of using biofuels could be the presence of impurities in the fuel, which will impact the durability of the aftertreatment catalysts of the vehicle. The presence of impurities in biogas is dependent on the feedstock, as this type of fuel can be produced

from several different feedstocks, causing different compositions of impurities in the final fuel. Some of the most potent catalyst poisons that could be present in the fuel and/or lubrication oil are sulfur, phosphorus, and siloxanes [4].

Bi-metallic Pd/Pt catalysts are today commonly used for oxidation of CO, HC, and NO in the aftertreatment system in vehicles [5,6]. The role of palladium in these catalysts is to be active for oxidation of methane; however, palladium based catalysts are sensitive to the presence of water vapor and tend to lose activity over time due to hydrothermal sintering [7–10]. As water is always present in the combustion exhaust, palladium based catalysts are often modified by the addition of platinum, which stabilizes the active metal particles and makes them less prone to sintering [11]. Besides sintering [12], oxidation catalysts may deactivate by other mechanisms [13–15], one of the most studied of which is SO₂ poisoning [16–19]. The bi-metallic catalysts can be deactivated by poisoning and sintering of precious metal particles similar to mono-metallic catalysts. However, the bi-metallic catalysts may in addition suffer from segregation of the metals as shown by Gremminger et al. The Pd/Pt bi-metallic catalyst is dynamic and presents surface species that are dependent on the reaction condition [20], and when exposed to water, these Pd/Pt species could segregate [21]. This segregation of platinum and palladium into mono-metallic particles impacts the stability and activity of the catalyst. Many studies are focused on a single poison at the lab scale [12,16–18,21,22], while others compare the impact of lab aging and vehicle aging [22–24].

In the present study, the impact of biogas exhaust on the oxidation catalyst performance is investigated. The exhaust exposure is conducted for 900 h in an engine bench setup with a full Euro VI emission control system. In that way, an understanding of how the use of biogas impacts the oxidation catalyst in a real-life exhaust environment can be achieved.

2. Results and Discussion

The catalyst samples used are named according to Table 1.

Table 1. Description of the catalyst samples.

Sample Name	Description
DOCref	Fresh sample of the oxidation catalyst
DOC in	Inlet sample of the engine bench aged oxidation catalyst
DOC out	Outlet sample of the engine bench aged oxidation catalyst

Figure 1a–c shows the conversion of CH₄, NO, and CO versus temperature using a feed consisting of the mentioned gases, water, oxygen, and argon as balance. Results are shown for the fresh Pd/Pt oxidation catalyst (DOC ref) and for an inlet (DOC in) and an outlet (DOC out) sample of the catalyst after 900 h aging with biogas exhaust in the engine bench. The performance of the samples was measured during heating and cooling ramps between 100 and 450 °C at a rate of 5 °C/min. The conversion performance of the catalysts to oxidize each of these compounds was also measured separately. The results for these experiments are shown in Figure 1d–f. From the results of the heating ramp experiments presented in Figure 1a,d, it is clear that the exposure to biogas exhaust results in a considerable decrease in the catalyst's ability to oxidize CH₄, in particular for the inlet part of the engine aged catalyst. It can also be observed that the complex gas mixture results in a higher conversion of CH₄ than what is obtained without CO and NO in the feed, as shown in Figure 1d and Table 2. The presence of NO during methane oxidation has been shown to be beneficial in studies by Sadokhina et al. [25]. These authors suggested that the improved activity originates from the reaction between NO and hydroxyl groups on the surface of the active phase, leaving more active sites available for methane oxidation.

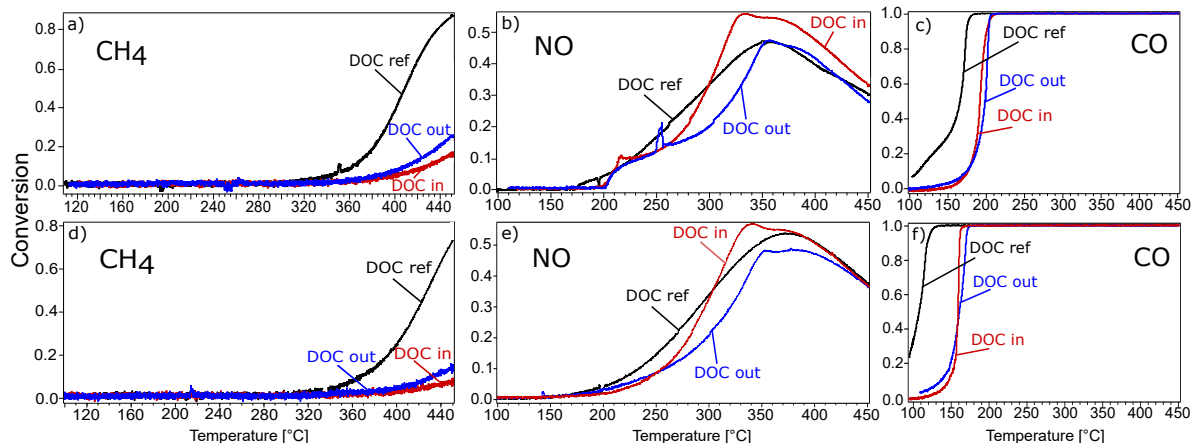


Figure 1. Conversion during heating of (a,d) CH₄, (b,e) NO and (c,f) CO over the fresh oxidation catalyst (DOC ref) and the inlet (DOC in) and outlet (DOC out) of the engine bench aged oxidation catalyst. Top row (a–c), in a feed consisting of 1000 ppm CH₄, 1000 ppm NO, 1000 ppm CO, 8% H₂O, 5% O₂, and argon as balance. Bottom row (d–f), in a feed consisting of 1000 ppm CH₄ or 1000 ppm NO or 1000 ppm CO with 8% H₂O, 5% O₂, and argon as balance.

Table 2. Conversion of methane at 450 °C for 50% conversion of CO (T₅₀) in a feed with and without NO and CO over the fresh oxidation catalyst (DOC ref) and the inlet (DOC in) and outlet (DOC out) of the engine bench aged oxidation catalyst.

Sample	Conversion of CH ₄ in the Presence of NO and CO (%)	Conversion of CH ₄ in Absence of NO and CO (%)	T ₅₀ for CO in the Presence of NO and CO (°C)	T ₅₀ for CO in the Absence of NO and CO (°C)
DOC ref	87	72	166	108
DOC in	15	8	192	159
DOC out	26	15	199	161

Downstream of the oxidation catalyst and the particulate filter in the emission control system is the selective catalytic reduction (SCR) catalyst, which reduces NO_x into nitrogen and water. The NO_x reduction can take place by several different routes depending on the NO/NO_x ratio [26]. The route that is desired is the fast-SCR reaction, which is followed when the NO/NO_x ratio is around 0.5. In Figure 1b,e, the conversion of NO to NO₂ over the oxidation catalyst is shown. At lower temperatures, the samples exposed to biogas exhaust show lower activity for oxidation of NO, when compared to the reference sample, in both gas mixtures, and the outlet part of the engine aged oxidation catalyst appears to have lost slightly more of its activity. However, at temperatures above 300 °C, the inlet sample of the aged oxidation catalyst shows a higher or similar conversion of NO in both gas compositions. It has been shown by Mulla et al. [27] that larger Pt particles are more active for oxidation of NO compared to smaller ones, and as seen from the TEM images in Figure 2, the noble metal particle size has increased after exposure of the oxidation catalyst to biogas exhaust, in particular for the inlet sample, due to sintering. Furthermore, a separation of the conversion maximum of NO into two peaks is visible for the samples exposed to biogas. This double peak could be caused by the segregation of Pd/Pt into mono-metallic sites. Platinum is more active for NO oxidation when compared to palladium, and as mentioned, large Pt particles are especially active for NO oxidation [28]. Hence, the double peak appears only for the engine bench aged samples where large mono-metallic Pt particles likely have formed and not for the fresh sample of the oxidation catalyst.

After exposure to biogas exhausts, the temperature where 50% conversion (T₅₀) of CO is reached is shifted 25 °C towards higher temperatures in the complex gas feed and 50 °C in the feed with only CO besides oxygen, water, and argon, see Table 2. For CO, the decrease in activity of the oxidation catalyst after exposure to biogas exhaust is evident from Figure 1c,f; however, the decrease in activity is not as severe as for CH₄. The impact of the other components in the complex feed on the conversion of

CO is clear when comparing Figure 1c and Figure 1f. In the presence of NO and methane, the activity for CO oxidation is significantly lower for both the fresh and the engine aged catalysts compared to the corresponding feed without CH₄ and NO (see Table 2).

The content of sulfur (S), phosphorus (P), and calcium (Ca) in the fresh and aged oxidation catalysts is shown in Table 3. The table also shows the composition of the catalyst in terms of Pt and Pd content; note that the reference sample has a slightly lower content of noble metals. This could be due to the fact that the fresh and engine aged samples come from different batches. The catalyst cores used in the engine bench setup are cut from longer cores produced by the catalyst manufacturer. There is a gradient in coating over the length of the catalyst, which could cause a difference in catalyst loading between the samples. It can be seen that S, P, and Ca are found in higher concentrations on the inlet sample of the engine bench aged oxidation catalyst compared to the corresponding outlet sample. It is also seen that the concentrations of S and P are substantially higher than the concentration of Ca. This is expected since the former two compounds are present in higher concentrations in both the fuel and the lubrication oil [29], while Ca is a component only present in the lubrication oil [23].

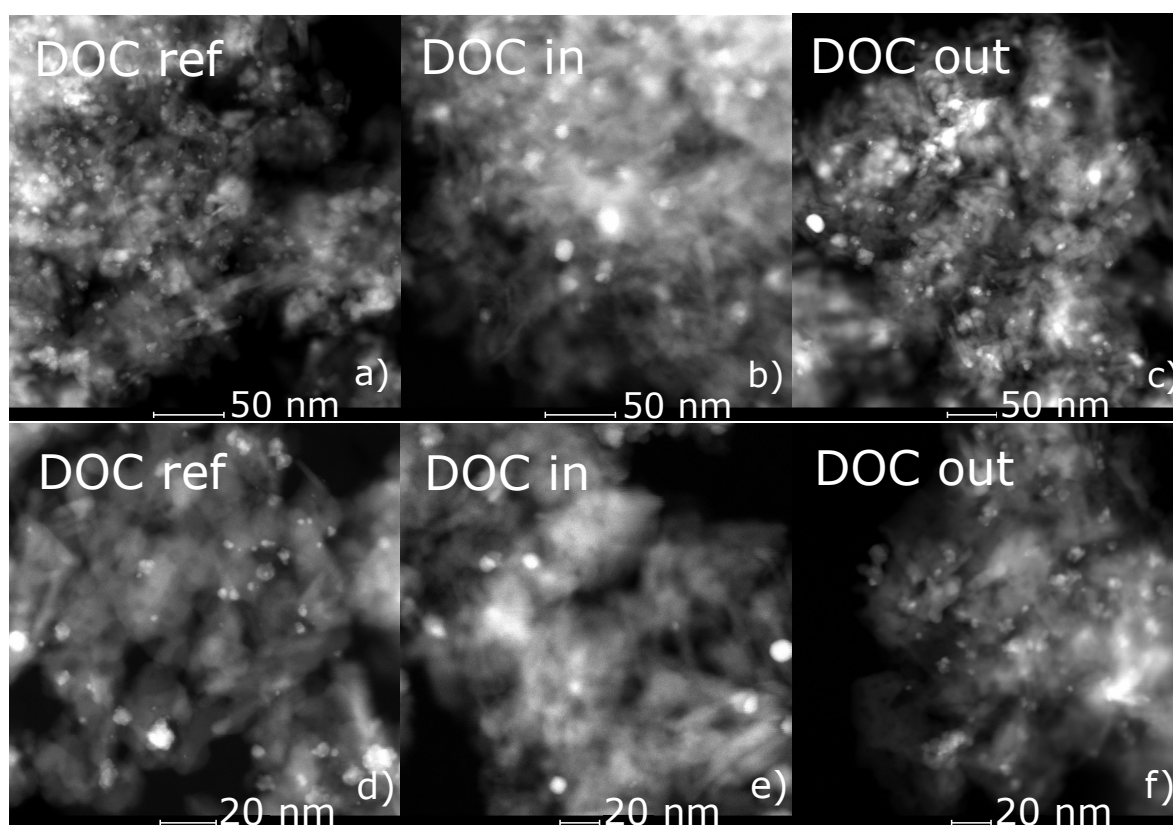


Figure 2. TEM images of (a,d) the fresh oxidation catalyst (DOC ref) and (b,e) the inlet (DOC in) and (c,f) outlet (DOC out) of the engine bench aged oxidation catalyst, at two magnifications, (a–c) and (d–f), respectively.

Table 3. Content of Pd, Pt, S, P, and Ca in the fresh oxidation catalyst (DOC ref) and in the inlet (DOC in) and outlet (DOC out) of the engine bench aged oxidation catalyst as obtained by XRF analysis.

Sample	Pd (wt.%)	Pt (wt.%)	S (wt.%)	P (wt.%)	Ca (ppm)
DOC ref	0.49 ± 0.05	0.20 ± 0.05	0.00 ± 0.04	0.00 ± 0.04	280 ± 70
DOC in	0.64 ± 0.05	0.24 ± 0.05	0.27 ± 0.04	0.18 ± 0.04	470 ± 70
DOC out	0.69 ± 0.05	0.27 ± 0.05	0.25 ± 0.04	0.04 ± 0.04	320 ± 70

In the TEM images, the Pt/Pd, Pt, and Pd particles are shown as bright dots, as can be seen in Figure 2. It is clear that the particle size has increased for the samples exposed to biogas exhaust

(Figure 2b,c,e,f). The average noble metal particle size was calculated on the basis of 100 particles, and the result is summarized in Table 4, where the particle size distribution is also included. The size of the active metal particles in the oxidation catalyst increased after exposure to biogas exhaust in the engine bench, likely due to thermal effects [23]. On the other hand, the temperature measured in the oxidation catalyst during aging did not exceed 550 °C, which means that sintering should not be severe. However, the presence of sulfur and phosphorus in the engine exhaust has been shown to promote sintering of Pt into larger particles [30,31]. The combination of long term exposure in an oxidizing environment at temperatures up to 550 °C, in combination with the presence of sulfur and phosphorus in the exhaust, is probably the cause of the observed sintering of Pt.

From the X-ray diffractograms shown in Figure 3, it is evident that the peak around 40 degrees (2θ) is shifted towards higher angles for the aged samples, in particular for the inlet sample of the engine bench aged oxidation catalyst. This indicates that the bimetallic catalyst has more mono-metallic sites, and in combination with the increased intensity of that peak, it is clear that there are larger mono-metallic particles present after aging of the catalyst [32–35]. The increased intensity is also seen for the Pd peak around 46.5 degrees, which is in agreement with the TEM analysis and activity tests, also showing that the particle size is increased and that more mono-metallic particles are present after exposure to biogas exhaust.

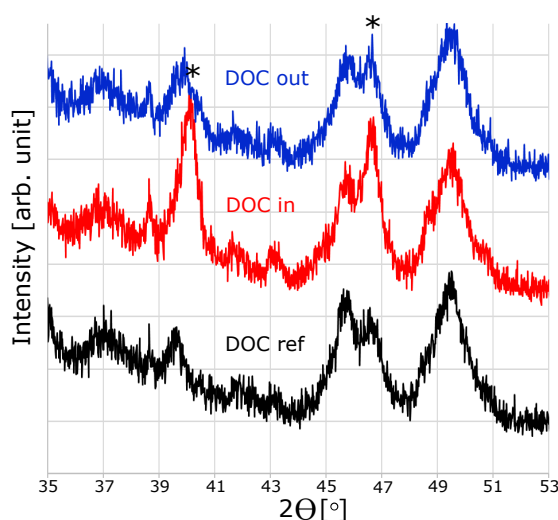


Figure 3. X-ray diffractograms for the fresh oxidation catalyst (DOC ref) and for the inlet (DOC in) and outlet (DOC out) of the engine bench aged oxidation catalyst. The diffraction patterns have been shifted in intensity for clarification, and full patterns between 30 and 90 degrees (2θ) can be found in the Supporting Information. Diffraction peaks indicated by * show Pd.

The poisoning by S and P indicated by the presence of these elements (see Table 3) and the increased Pd/Pt particle size (Figure 2) will cause blocking and loss of active sites, respectively. The blocking and loss of active sites can clearly be seen from the CO chemisorption measurements presented in Table 4. The amount of CO that is chemisorbed on equimolar amounts of noble metal strongly decreases for the samples that have been exposed to biogas exhaust for 900 h in the engine bench compared to the reference sample of the oxidation catalyst.

Table 4. Average Pd/Pt metal particle size, particle size distribution, and CO uptake for the fresh oxidation catalyst (DOC ref) and for the inlet (DOC in) and outlet (DOC out) of the engine bench aged oxidation catalyst as obtained by TEM and CO chemisorption.

Sample	Average Noble Metal Particle Size (nm)	Particle Size Distribution (nm)	CO Uptake (mol/mol Pd/Pt)
DOC ref	4.0	2–9	0.063
DOC in	9.5	5–17	0.001
DOC out	8.0	2–19	0.003

Table 3 indicates that sulfur is uniformly distributed over the length of the engine bench aged oxidation catalyst, while phosphorus is found in higher concentrations in the inlet of the catalyst, in agreement with previous studies [13,36,37]. This could also be seen from the SEM-EDX analysis (Figure 4) where phosphorus is mapped in yellow. The concentration of P is clearly higher on the surface of the washcoat for the inlet sample of the engine bench aged oxidation catalyst, while S is more evenly distributed over the washcoat, as well as the length of the catalyst [38]. The increased concentration of P on the inlet sample of the engine bench aged oxidation catalyst, when compared to the corresponding outlet sample, results in fewer available active sites. This, together with the loss of active sites due to Pd/Pt sintering, could explain the measured difference in activity for methane oxidation for the fresh and aged samples; see Figure 1a,d.

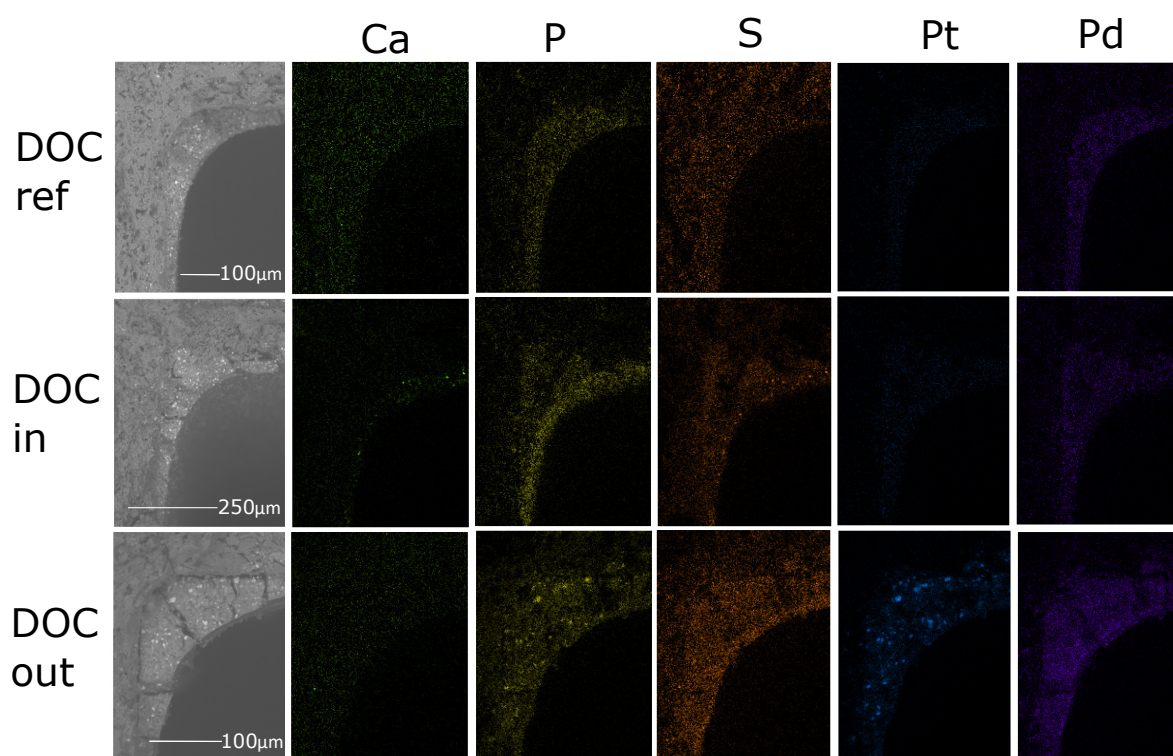


Figure 4. SEM images and EDX maps of Ca, P, S, Pt, and Pd for the fresh oxidation catalyst (DOC ref) and for the inlet (DOC in) and outlet (DOC out) of the engine bench aged oxidation catalyst.

From the XPS analysis, it is clear that several elements are present on the surface of the samples. The survey spectra with assigned peaks for Pd, Pt, Al, Si, C, and O are included in the Supporting Information (see Figures A1 and A2) for clarification. From the XPS spectra shown in Figure 5 (left column), we found that phosphorus is present in the inlet sample of the engine bench aged oxidation catalyst in two different forms, as phosphate (135 eV) and oxidized phosphorus (likely at 138 eV) [39]. P_4O_{10} , also known as phosphate glass, covers the surface of the sample in a non-selective way, while the phosphates could form bonds with the alumina support [40,41]. For the outlet sample

of the engine bench aged oxidation catalyst, mainly phosphate is found, and this is most likely due to P_4O_{10} sticking to the first surface it comes in contact with, which is the inlet of the oxidation catalyst. From the XPS analysis, we can also see that sulfur is present in the form of sulfate on both engine bench aged samples. Sulfates primarily form $PdSO_4$ at ambient pressure, and no or minor formation of $PtSO_4$ is expected [42,43]. In agreement with the XRF analysis, neither sulfur nor phosphorus is found on the reference sample

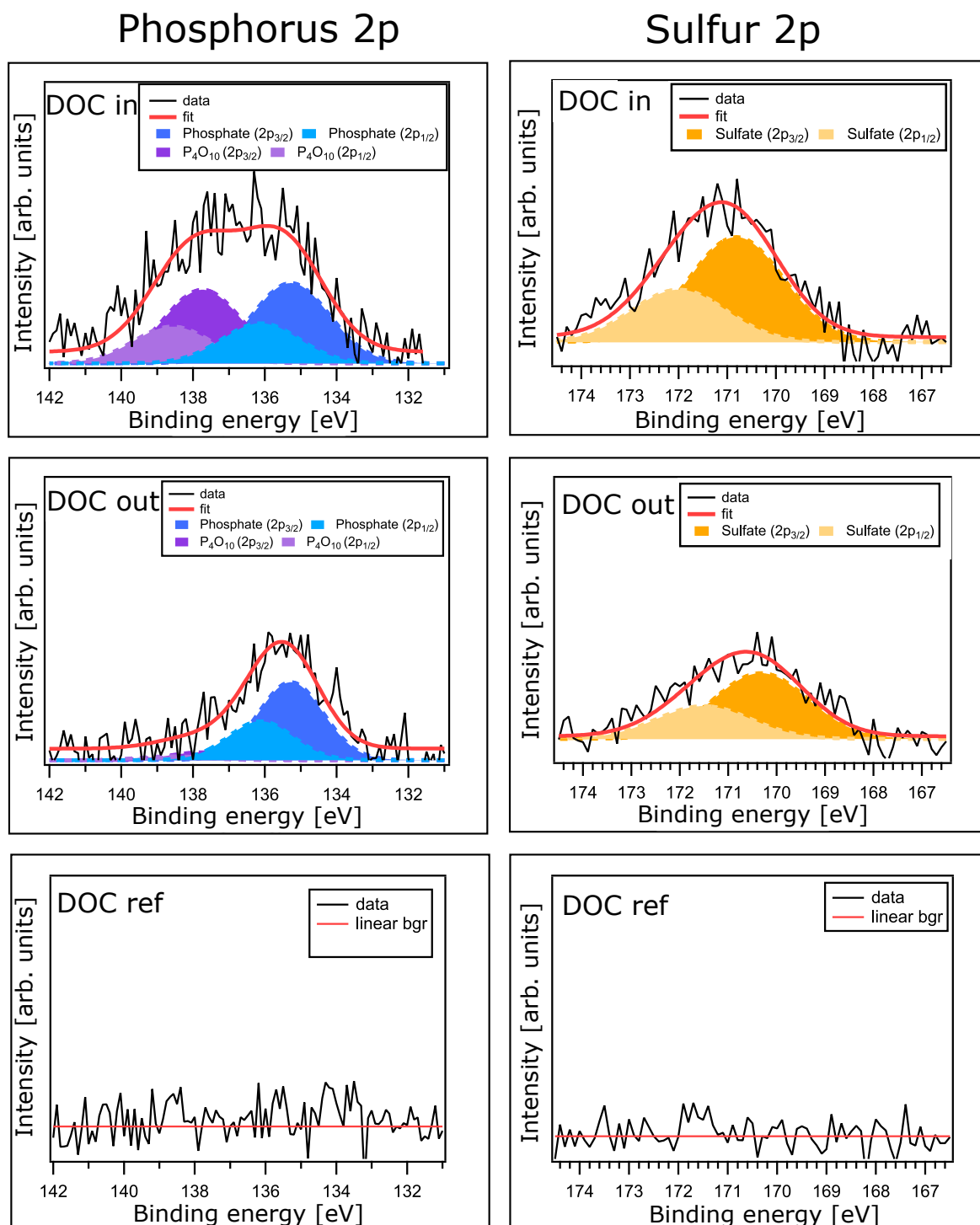


Figure 5. Phosphorus and sulfur 2p core level spectra of the fresh oxidation catalyst (DOC ref) and of the inlet (DOC in) and outlet (DOC out) of the engine bench aged oxidation catalyst.

3. Materials and Methods

The aging of the catalysts was performed in an engine bench consisting of a Volvo G13C 460 hp engine and a Euro VI emission control system, and the setup is schematically shown in Figure 6. The engine was a dual-fuel type engine, which was powered with 90% biogas and 10% diesel for 900 h, during which the gas flow was altered to simulate mixed driving. The temperature in the engine bench was kept between 170 and 550 °C throughout the duration of the aging. After exposure to biogas exhausts for 900 h, the emission control system was dismantled, and the parts were characterized and tested separately.

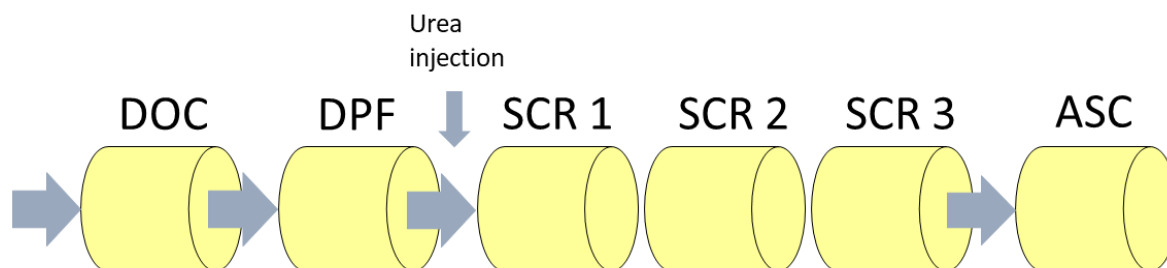


Figure 6. Emission control system setup with the oxidation catalyst (DOC), particulate filter (DPF), selective catalytic reduction (SCR) catalysts (SCR 1-3), and ammonia slip catalyst (ASC).

3.1. Catalyst Material

The oxidation catalyst used in this study was a Pd/Pt based catalyst supported on alumina (Al_2O_3) and washcoated onto a cordierite substrate. The catalyst samples were provided by a catalyst manufacturer, and no further specification of the sample preparation procedure is available. Full size bricks were used in the engine bench while sample cores with a diameter 11 mm and a length 19 mm were drilled out and tested in the synthetic gas bench reactor. The noble metal loading of the catalyst was 100 g/ft³, and the Pt:Pd ratio was 1:2 by weight. Samples were taken from the inlet and the outlet of the oxidation catalyst to observe any axial differences downstream of the catalyst. The engine bench aged samples of the oxidation catalyst were compared with a fresh sample. The cell density of the oxidation catalyst was 400 cpsi.

3.2. Activity Testing

The catalyst activity during CO, CH₄, and NO oxidation was evaluated in a synthetic gas bench reactor. The activity of the catalyst (DOC) to oxidize each gaseous compound was evaluated separately, as well as in a complex mixture. The experimental conditions are shown in Table 5. The synthetic gas bench reactor, described in detail elsewhere [44], consisted of a horizontal quartz tube heated by a resistive heating coil. The gas flow was controlled by Hi-Tech Bronkhorst mass flow controllers. The water was fed by a Bronkhorst CEM system, and the effluent gases were analyzed by an MKS 2030 HS Fourier transform infrared spectrometer (FTIR). Thermocouples were placed in a blank monolith substrate upstream of the oxidation catalyst for temperature control and in the center of the oxidation catalyst for temperature monitoring.

3.3. Characterization

3.3.1. SEM-EDX

The radial distribution and position of elements were mapped using a Hitachi SU-500 scanning electron microscope (SEM, AB Volvo, Gothenburg, Sweden) equipped with an energy-dispersive X-ray (EDX, AB Volvo, Gothenburg, Sweden) analysis system, Oxford Instruments SDD 80 mm². Full cores were cut from the fresh and engine bench aged samples, and 10 mm thick slices were cut from the cores, then the untreated uncut surface was analyzed.

Table 5. Experimental protocol for oxidation activity tests. Base feed for all experiments: 8 vol.% O₂, 5 vol.% H₂O, and Ar used as balance. GHSV: 45,000 h^{−1}. The temperature was increased and decreased linearly by 5 °C/min.

Temp (°C)	CO (vol. ppm)	CH ₄ (vol. ppm)	NO (vol. ppm)	Description
100–450↑↓	1000	-	-	CO oxidation
100–450↑↓	-	1000	-	CH ₄ oxidation
100–450↑↓	-	-	1000	NO oxidation
100–450↑↓	1000	1000	1000	Complex mixture of gases

3.3.2. Elemental Analysis Using XRF

A PANalytical Epsilon 3XL analyzer (Scania CV, Södertälje, Sweden and Chalmers University of Technology, Gothenburg, Sweden) was used to perform X-ray fluorescence (XRF) analysis to determine semi-quantitatively the elemental composition of the fresh and engine bench aged catalyst samples. For the analysis, around 2 g of each of the samples was needed, and the washcoat and cordierite substrate were analyzed together. The samples were mixed with a binder using a ball mill (300 rpm, 10 min) and then pressed into flat briquettes (150 kN, 3 min). This method does not quantify the amount of catalyst poisons in the samples exactly, but for comparison of poison content between similar samples, the method is satisfying. The measurement was performed three times to receive an error margin.

3.3.3. TEM

Transmission electron microscopy (TEM) was performed using an FEI Titan 80–300 instrument operating at an accelerating voltage of 300 kV (Chalmers University of Technology, Gothenburg, Sweden). Images were acquired in the scanning TEM (STEM) mode using a high angle annular dark field (HAADF) detector. The average noble metal particle size and the particle size distribution for each catalyst sample were determined from these images. A small amount of washcoat was scraped off from the monolith sample and transferred to a copper grid. Images were recorded at several different magnifications for each sample.

3.3.4. XRD

XRD (X-ray diffraction) was used to determine if segregation of Pd and Pt occurred during engine bench aging. The X-ray diffractometer used was a Bruker axs D8 ADVANCE instrument (Chalmers University of Technology, Gothenburg, Sweden) with a Cu K α radiation equivalent to 0.15418 nm. The washcoat was scraped off, and the powder sample was transferred to a sample holder with a silicon wafer as the base. Diffraction data were collected for $2\theta = 30\text{--}90^\circ$.

3.3.5. XPS

The presence and chemical state of the elements on the surface of the catalyst samples were identified by X-ray photoelectron spectroscopy (XPS) using a VersaProbe III Scanning XPS Microprobe (Chalmers University of Technology, Gothenburg, Sweden) with an Al anode providing monochromated K α radiation (1486.6 eV). For charge compensation, both an ion gun (Ar⁺) and electron neutralizer (e[−]) were used. The sample was prepared by cutting out six channels from the monolith core and attaching them by using double sided carbon tape. The analyzed area was $500 \times 500 \mu\text{m}^2$, and the information depth was around 5 nm. The binding energy scale was calibrated to the position of the Si 2p signal of SiO₂ at 103.3 eV [45], because the nature of the varying amount of carbon present on the different samples could not be determined with certainty, and hence, calibration to the carbon signal was unreliable. We estimated an accuracy of ± 0.5 eV for the binding energy. The spectra were normalized to the background at the low binding energy end. The P 2p and S 2p spectra in Figure 5

were deconvoluted using a Voigt profile with a spin-orbit split of $\Delta = 0.85$ eV for P 2p and $\Delta = 1.18$ eV for S 2p, respectively [45]. A linear background was subtracted prior to deconvolution.

3.3.6. CO Chemisorption

To quantify the active sites on the catalyst, CO chemisorption was performed using an ASAP2020 instrument from Micromeritics (Chalmers University of Technology, Gothenburg, Sweden). The samples were prepared by cutting out 3×3 channels from each catalyst sample. The sample was then confined between folded quartz wool and oxidized at 350 °C for 1 h followed by evacuation for 15 min and reduction by hydrogen at 350 °C for 1 h. The pretreatment was finalized by evacuation at 350 and 35 °C for 10 min each. The CO chemisorption measurement was performed at 35 °C by gradually increasing the CO dosage from 100 to 600 mm Hg.

3.4. Biogas

Biogas refers to gases produced by anaerobic fermentation or digestion of organic matter like sewage waste [46]. The biogas used for aging in this study follows European standards, which means that the concentrations of impurities like sulfur are limited. The total sulfur content in biogas, excluding odorant, should be below 20 mg/m³ [47].

4. Conclusions

The exhaust from a dual-fuel heavy-duty engine powered by biogas and equipped with a Euro VI emission control system was shown to have a significant impact on the CH₄ oxidation activity of the Pd/Pt bimetallic oxidation catalyst. We could also observe that the activity for CO oxidation decreased while the activity for NO oxidation increased for the inlet of the oxidation catalyst after 900 h of exposure to biogas exhausts. The loss of activity for CH₄ and CO oxidation was likely caused by loss of active sites by sintering and poisoning by sulfur and phosphorus. The explanation for the increased NO oxidation at higher temperatures was that larger Pt particles had higher activity for oxidation of NO to NO₂. Evidence of sintering was seen in the results from TEM and XRD analysis, and indications of sintering/poisoning could be seen in the decrease in CO uptake during CO chemisorption for the aged catalyst. The presence of catalyst poisons, i.e., S and P, was confirmed by XRF, XPS, and SEM-EDX. The distribution of sulfur was uniform throughout the washcoat and the length of the aged oxidation catalyst, while higher concentrations of phosphorus were seen on the surface of the washcoat and in the inlet of the catalyst. Sulfur was present in the form of sulfates, which mainly react with Pd sites. Phosphorus, however, was found in two different states where the P₄O₁₀ state was only found in the inlet of the aged catalyst, while phosphates were present both in the inlet and outlet of the aged catalyst. Both phosphorus states covered the surface, and the phosphate could also react with the alumina support. To ensure a good transition from the use of fossil fuels to more bio based fuels, optimization of the oxidation catalyst is needed, in particular for the oxidation of methane.

Author Contributions: Conceptualization, L.J.P. and M.S.; Data curation, J.E., D.J., A.S. and S.D.; Formal analysis, J.E., D.J., S.D., A.S., L.J.P. and M.S.; Funding acquisition, L.J.P. and M.S.; Investigation, J.E. and K.X.; Methodology, J.E., K.X., S.S., L.A., L.J.P. and M.S.; Project administration, J.E.; Resources, K.X., D.J., S.D., A.S., S.S. and L.A.; Supervision, K.X., S.S., L.A., P.-A.C., L.J.P. and M.S.; Visualization, J.E.; Writing—original draft, J.E.

Funding: This work was financially supported by the Swedish Energy Agency through the FFI program (No: 38364-1) and the Competence Centre for Catalysis, which is financially supported by Chalmers University of Technology, the Swedish Energy Agency, and the member companies AB Volvo, ECAPS AB, Johnson Matthey AB, Preem AB, Scania CV AB, Umicore Denmark ApS, and Volvo Car Corporation AB.

Conflicts of Interest: The authors declare no conflict of interest.

Appendix A.

Appendix A.1. XRD

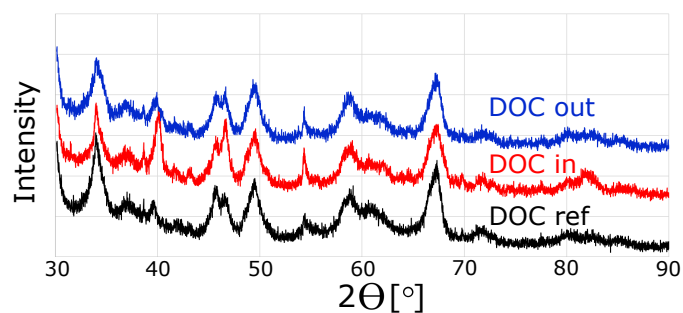


Figure A1. Full XRD diffractograms for the fresh (DOC ref) and the inlet of the engine bench aged (DOC in) and outlet (DOC out) of the engine bench aged oxidation catalyst.

Appendix A.2. XPS

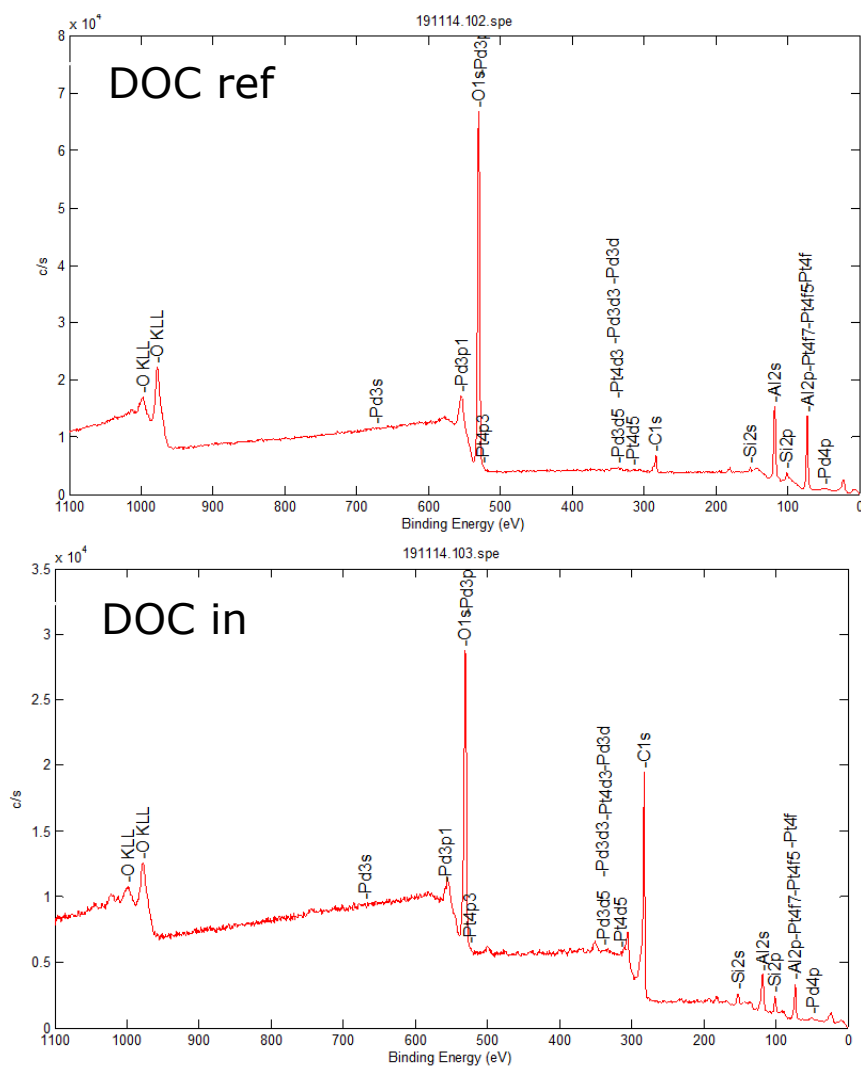


Figure A2. Cont.

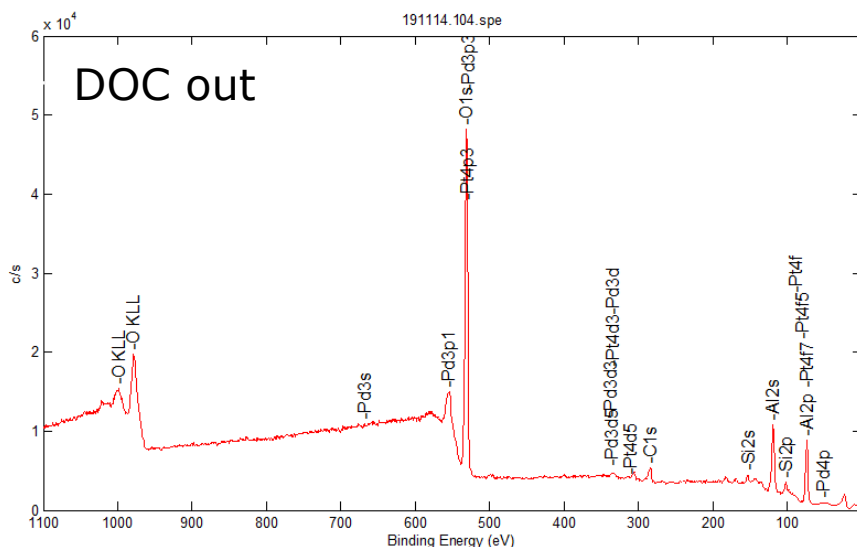


Figure A2. Full XPS survey spectra for the fresh oxidation catalyst (DOC ref) and the inlet (DOC in) and outlet (DOC out) of the engine bench aged oxidation catalyst.

References

1. Regulation (EU) 2019/631. *Off. J. Eur. Union* **2019**. Available online: <https://eur-lex.europa.eu/eli/reg/2019/631/oj> (accessed on 9 October 2019).
2. Regulations No 595/2009. *Off. J. Eur. Union* **2009**. Available online: <https://eur-lex.europa.eu/eli/reg/2009/595/oj> (accessed on 9 October 2019).
3. Binder, A.J.; Toops, T.J.; Unocic, R.R.; Parks, J.E., II; Dai, S. Low-Temperature CO Oxidation over a Ternary Oxide Catalyst with High Resistance to Hydrocarbon Inhibition. *Angew. Chem. Int. Ed.* **2015**, *54*, 13263–13267. [[CrossRef](#)] [[PubMed](#)]
4. Chiodo, V.; Maisano, S.; Zafarana, G.; Urbani, F. Effect of pollutants on biogas steam reforming. *Int. J. Hydrog. Energy* **2017**, *42*, 1622–1628. [[CrossRef](#)]
5. Martin, N.M.; Nilsson, J.; Skoglundh, M.; Adams, E.C.; Wang, X.; Smedler, G.; Raj, A.; Thompsett, D.; Agostini, G.; Carlson, S.; et al. Study of methane oxidation over alumina supported Pd–Pt catalysts using operando DRIFTS/MS and in situ XAS techniques. *Catal. Struct. React.* **2017**, *3*, 24–32. [[CrossRef](#)]
6. Martin, N.M.; Skoglundh, M.; Smedler, G.; Raj, A.; Thompsett, D.; Velin, P.; Martinez-Casado, F.J.; Matej, Z.; Balmes, O.; Carlsson, P.A. CO Oxidation and Site Speciation for Alloyed Palladium–Platinum Model Catalysts Studied by in Situ FTIR Spectroscopy. *J. Phys. Chem. C* **2017**, *121*, 26321–26329. [[CrossRef](#)]
7. Lapisardi, G.; Urfels, L.; Gélín, P.; Primet, M.; Kaddouri, A.; Garbowski, E.; Toppi, S.; Tena, E. Superior catalytic behaviour of Pt-doped Pd catalysts in the complete oxidation of methane at low temperature. *Catal. Today* **2006**, *117*, 564–568. [[CrossRef](#)]
8. Ersson, A.; Kušar, H.; Carroni, R.; Griffin, T.; Järås, S. Catalytic combustion of methane over bimetallic catalysts a comparison between a novel annular reactor and a high-pressure reactor. *Catal. Today* **2003**, *83*, 265–277. [[CrossRef](#)]
9. Kinnunen, N.M.; Hirvi, J.T.; Suvanto, M.; Pakkanen, T.A. Methane combustion activity of Pd–PdOx–Pt/Al₂O₃ catalyst: The role of platinum promoter. *J. Mol. Catal. A Chem.* **2012**, *356*, 20–28. [[CrossRef](#)]
10. Morlang, A.; Neuhausen, U.; Klementiev, K.; Schütze, F.W.; Miehe, G.; Fuess, H.; Lox, E. Bimetallic Pt/Pd diesel oxidation catalysts: Structural characterisation and catalytic behaviour. *Appl. Catal. B Environ.* **2005**, *60*, 191–199. [[CrossRef](#)]
11. Honkanen, M.; Kärkkäinen, M.; Viitanen, V.; Jiang, H.; Kallinen, K.; Huuhtanen, M.; Vippola, M.; Lahtinen, J.; Keiski, R.; Lepistö, T. Structural Characteristics of Natural-Gas-Vehicle-Aged Oxidation Catalyst. *Top. Catal.* **2013**, *56*, 576–585. [[CrossRef](#)]
12. González-Velasco, J.R.; Botas, J.A.; Ferret, R.; González-Marcos, M.P.; Marc, J.L.; Gutiérrez-Ortiz, M.A. Thermal aging of Pd/Pt/Rh automotive catalysts under a cycled oxidizing–reducing environment. *Catal. Today* **2000**, *59*, 395–402. [[CrossRef](#)]

13. Neyestanaki, A.K.; Klingstedt, F.; Salmi, T.; Murzin, D.Y. Deactivation of postcombustion catalysts, a review. *Fuel* **2004**, *83*, 395–408. [CrossRef]
14. Forzatti, P.; Lietti, L. Catalyst deactivation. *Catal. Today* **1999**, *52*, 165–181. [CrossRef]
15. Kim, J.; Kim, Y.; Wiebenga, M.H.; Oh, S.H.; Kim, D.H. Oxidation of C₃H₈, iso-C₅H₁₂ and C₃H₆ under near-stoichiometric and fuel-lean conditions over aged Pt–Pd/Al₂O₃ catalysts with different Pt:Pd ratios. *Appl. Catal. B Environ.* **2019**, *251*, 283–294. [CrossRef]
16. Corro, G.; Cano, C.; Fierro, J. A study of Pt–Pd/ γ -Al₂O₃ catalysts for methane oxidation resistant to deactivation by sulfur poisoning. *J. Mol. Catal. A Chem.* **2010**, *315*, 35–42. [CrossRef]
17. Mowery, D.L.; McCormick, R.L. Deactivation of alumina supported and unsupported PdO methane oxidation catalyst: The effect of water on sulfate poisoning. *Appl. Catal. B Environ.* **2001**, *34*, 287–297. [CrossRef]
18. Ordóñez, S.; Hurtado, P.; Sastre, H.; Díez, F. Methane catalytic combustion over Pd/Al₂O₃ in presence of sulphur dioxide: Development of a deactivation model. *Appl. Catal. A Gen.* **2004**, *259*, 41–48. [CrossRef]
19. Colussi, S.; Arosio, F.; Montanari, T.; Busca, G.; Groppi, G.; Trovarelli, A. Study of sulfur poisoning on Pd/Al₂O₃ and Pd/CeO₂/Al₂O₃ methane combustion catalysts. *Catal. Today* **2010**, *155*, 59–65. [CrossRef]
20. Martin, N.M.; Nilsson, J.; Skoglundh, M.; Adams, E.C.; Wang, X.; Velin, P.; Smedler, G.; Raj, A.; Thompson, D.; Brongersma, H.H.; et al. Characterization of Surface Structure and Oxidation/Reduction Behavior of Pd–Pt/Al₂O₃ Model Catalysts. *J. Phys. Chem. C* **2016**, *120*, 28009–28020. [CrossRef]
21. Gremminger, A.T.; de Carvalho, H.W.P.; Popescu, R.; Grunwaldt, J.D.; Deutschmann, O. Influence of gas composition on activity and durability of bimetallic Pd–Pt/Al₂O₃ catalysts for total oxidation of methane. *Catal. Today* **2015**, *258*, 470–480. [CrossRef]
22. Dahlin, S.; Lantto, C.; Englund, J.; Westerberg, B.; Regali, F.; Skoglundh, M.; Pettersson, L.J. Chemical aging of Cu-SSZ-13 SCR catalysts for heavy-duty vehicles—Influence of sulfur dioxide. *Catal. Today* **2019**, *320*, 72–83. [CrossRef]
23. Andersson, J.; Antonsson, M.; Eurenus, L.; Olsson, E.; Skoglundh, M. Deactivation of diesel oxidation catalysts: Vehicle- and synthetic aging correlations. *Appl. Catal. B Environ.* **2007**, *72*, 71–81. [CrossRef]
24. Wiebenga, M.H.; Kim, C.H.; Schmiege, S.J.; Oh, S.H.; Brown, D.B.; Kim, D.H.; Lee, J.H.; Peden, C.H. Deactivation mechanisms of Pt/Pd-based diesel oxidation catalysts. *Catal. Today* **2012**, *184*, 197–204. [CrossRef]
25. Sadokhina, N.; Smedler, G.; Nylén, U.; Olofsson, M.; Olsson, L. The influence of gas composition on Pd-based catalyst activity in methane oxidation—Inhibition and promotion by NO. *Appl. Catal. B Environ.* **2017**, *200*, 351–360. [CrossRef]
26. Devadas, M.; Kröcher, O.; Elsener, M.; Wokaun, A.; Söger, N.; Pfeifer, M.; Demel, Y.; Mussmann, L. Influence of NO₂ on the selective catalytic reduction of NO with ammonia over Fe-ZSM5. *Appl. Catal. B Environ.* **2006**, *67*, 187–196. [CrossRef]
27. Mulla, S.; Chen, N.; Cumarantunge, L.; Blau, G.; Zemlyanov, D.; Delgass, W.; Epling, W.; Ribeiro, F. Reaction of NO and O₂ to NO₂ on Pt: Kinetics and catalyst deactivation. *J. Catal.* **2006**, *241*, 389–399. [CrossRef]
28. Dubbe, H.; Bühner, F.; Eigenberger, G.; Nieken, U. Hysteresis Phenomena on Platinum and Palladium-based Diesel Oxidation Catalysts (DOCs). *Emiss. Control. Sci. Technol.* **2016**, *2*, 137–144. [CrossRef]
29. Jääskeläinen, H. *Impact of Engine Oil on Emissions and Fuel Economy*; Dieselnet: 2015. Available online: https://www.dieselnet.com/tech/lube_emissions.php (accessed on 9 October 2019).
30. Fridell, E.; Amberntsson, A.; Olsson, L.; Grant, A.W.; Skoglundh, M. Platinum oxidation and sulphur deactivation in NO_x storage catalysts. *Top. Catal.* **2004**, *30*, 143–146. [CrossRef]
31. Winkler, A.; Ferri, D.; Aguirre, M. The influence of chemical and thermal aging on the catalytic activity of a monolithic diesel oxidation catalyst. *Appl. Catal. B Environ.* **2009**, *93*, 177–184. [CrossRef]
32. Martin-Martinez, M.; Gómez-Sainero, L.; Bedia, J.; Arevalo-Bastante, A.; Rodriguez, J. Enhanced activity of carbon-supported Pd–Pt catalysts in the hydrodechlorination of dichloromethane. *Appl. Catal. B Environ.* **2016**, *184*, 55–63. [CrossRef]
33. Persson, K.; Ersson, A.; Colussi, S.; Trovarelli, A.; Järås, S. Catalytic combustion of methane over bimetallic Pd–Pt catalysts: The influence of support materials. *Appl. Catal. B Environ.* **2006**, *66*, 175–185. [CrossRef]
34. Rodríguez-Proenza, C.; Palomares-Báez, J.; Chávez-Rojas, M.; García-Ruiz, A.; Azanza Ricardo, C.; Santoveña-Urbe, A.; Luna-Barcenas, G.; Rodríguez-López, J.; Esparza, R. Atomic Surface Segregation and Structural Characterization of PdPt Bimetallic Nanoparticles. *Materials* **2018**, *11*, 1882. [CrossRef] [PubMed]

35. Esparza, R.; Santoveña, A.; Ruíz-Baltazar, A.; Angeles-Pascual, A.; Bahena, D.; Maya-Cornejo, J.; Ledesma-García, J.; Perez-Campos, R. Study of PtPd Bimetallic Nanoparticles for Fuel Cell Applications. *Mater. Res.* **2017**. [[CrossRef](#)]
36. Corro, G. Sulfur impact on diesel emission control—A review. *React. Kinet. Catal. Lett.* **2002**, *75*, 89–106. [[CrossRef](#)]
37. Haaß, F.; Fuess, H. Structural Characterization of Automotive Catalysts. *Adv. Eng. Mater.* **2005**, *7*, 899–913. [[CrossRef](#)]
38. Cabello Galisteo, F.; Larese, C.; Mariscal, R.; Granados, M.; Fierro, J.; Fernández Ruiz, R.; Furió, M. Deactivation on Vehicle-Aged Diesel Oxidation Catalysts. *Top. Catal.* **2004**, *30–31*, 451–456. [[CrossRef](#)]
39. Sherwood, P.M.A. Introduction to Studies of Phosphorus-Oxygen Compounds by XPS. *Surf. Sci. Spectra* **2002**, *9*, 62–66. [[CrossRef](#)]
40. Kärkkäinen, M.; Kolli, T.; Honkanen, M.; Heikkinen, O.; Väliheikki, A.; Huuhtanen, M.; Kallinen, K.; Lahtinen, J.; Vippola, M.; Keiski, R.L. The Influence of Phosphorus Exposure on a Natural-Gas-Oxidation Catalyst. *Top. Catal.* **2016**, *59*, 1044–1048. [[CrossRef](#)]
41. Eaton, S.J.; Nguyen, K.; Bunting, B.G. Deactivation of Diesel Oxidation Catalysts by Oil-Derived Phosphorus. Powertrain & Fluid Systems Conference and Exhibition. *SAE Int.* **2006**. [[CrossRef](#)]
42. Sharma, H.N.; Sharma, V.; Mhadeshwar, A.B.; Ramprasad, R. Why Pt Survives but Pd Suffers From SO_x Poisoning? *J. Phys. Chem. Lett.* **2015**, *6*, 1140–1148. [[CrossRef](#)]
43. Wilburn, M.S.; Epling, W.S. SO₂ adsorption and desorption characteristics of bimetallic Pd-Pt catalysts: Pd:Pt ratio dependency. *Catal. Today* **2019**, *320*, 11–19. [[CrossRef](#)]
44. Kannisto, H.; Ingelsten, H.H.; Skoglundh, M. Ag–Al₂O₃ catalysts for lean NO_x reduction—Influence of preparation method and reductant. *J. Mol. Catal. A Chem.* **2009**, *302*, 86–96. [[CrossRef](#)]
45. Moulder, J.F.; Stickle, W.F.; E. Sobol, P.; Bomben, K.D. *Handbook of X-ray Photoelectron Spectroscopy*; Perkin-Elmer Corporation: Eden Prairie, MN, USA, 1992.
46. Granstrand, J.; Dahlin, S.; Immele, O.; Schmalhorst, L.; Lantto, C.; Nilsson, M.; París, R.S.; Regali, F.; Pettersson, L.J. Catalytic aftertreatment systems for trucks fueled by biofuels—Aspects on the impact of fuel quality on catalyst deactivation. *RSC Catal.* **2018**, *30*, 64–145. [[CrossRef](#)]
47. CEN-CENELEC. EN 16726:2015. 2015. Available online: https://infostore.saiglobal.com/preview/98703699482.pdf?sku=879417_saig_nsai_nsai_2089598 (accessed on 9 October 2019).



© 2019 by the authors. Licensee MDPI, Basel, Switzerland. This article is an open access article distributed under the terms and conditions of the Creative Commons Attribution (CC BY) license (<http://creativecommons.org/licenses/by/4.0/>).